




RESEARCH ARTICLE OPEN ACCESS

Light-Soaking Effects in High-Efficiency Cu(In,Ga)Se₂ and (Ag,Cu)(In,Ga)Se₂ Solar Cells

Klara Kiselman¹  | Jan Keller¹  | Patrick Pearson¹ | Kostiantyn Sopiha¹  | Erik Wallin² | Marika Edoff¹¹Division of Solar Cell Technology, Department of Materials Science and Engineering, Uppsala University, Uppsala, Sweden | ²First Solar European Technology Center, Uppsala, Sweden**Correspondence** Klara Kiselman (klara.kiselman@angstrom.uu.se)**Received:** 21 November 2024 | **Revised:** 3 March 2025 | **Accepted:** 27 March 2025**Funding:** This research was supported by the Swedish Energy Agency through the projects "Solar Electricity Research Center (SOLVE)", Project no 52693-1, and "Advanced optical concepts in ACIGS solar cells", Project no 43523-2.**Keywords:** (Ag | Cu)(In | Ga)Se₂ | Cu(In | Ga)Se₂ | external radiative efficiency | light-soaking | metastability | photoluminescence

ABSTRACT

Metastable behaviours with respect to light-soaking of Cu(In,Ga)Se₂ (CIGS) solar cells have long been known and studied, but no explanation has yet been fully agreed on. In this study, silver alloying and its impact on light-soaking effects is explored in four CIGS and six (Ag,Cu)(In,Ga)Se₂ (ACIGS) samples with high efficiency (17% to 21% before light-soaking). All were produced by co-evaporation and similar depositions protocols as the current world record device but with some variation. A variety of opto-electronic characterisation methods were used to explore the response to 24 h of light-soaking at 50°C. We found that (i) the open-circuit voltage increased for all ACIGS devices but decreased for the CIGS devices, (ii) the cells entered a state with higher doping and more tail states, and (iii) the effect was metastable and partially reverted after dark storage. While the improvement of the ACIGS cells saturates after 24 h in one-third of the irradiance at one sun, months are needed to reverse the open-circuit voltage change. Despite a higher doping after light-soaking, none of the samples' short-circuit current showed significant changes and the efficiency after light-soaking ranged from 15% to 22%. No long-range change in sodium or rubidium distributions was observed using glow-discharge optical emission spectroscopy. In general, external radiative efficiency measurements showed that the nonradiative recombination loss is reduced after light-soaking in the ACIGS devices. However, the correlation to the measured voltage was not always straight forward, presumably due to the graded bandgap of the absorber.

1 | Introduction

As the world truly embarks on the transition to a sustainable energy production, the need for more renewable energy sources increases. Photovoltaics are key contributors to this transition, and some important traits are high efficiencies and long-term stability. For thin-film solar cells based on Cu(In,Ga)Se₂ (CIGS) alloyed with silver to (Ag,Cu)(In,Ga)Se₂ (ACIGS), the record power conversion efficiency is 23.6% [1]. While CIGS solar cells have already been commercialised with a guarantee of 80% of the power production after 25 years, metastable light-soaking (LS)-induced phenomena have been known for a long time and

may impact the reliability. The effect of LS on ACIGS was recently particularly highlighted when the current record device reached its certified efficiency after 24 h of LS. In this study, we build upon the light-soaking of the record device by analysing 10 high efficiency (>17%) CIGS and ACIGS devices produced with similar routines as the record 23.6% cell.

Silver alloying of CIGS has in recent years increased in popularity and the two most recent efficiency records both used different amount of silver. Solar frontier reached 23.35% in 2019 with an [Ag]/([Ag]+[Cu]) (AAC) ratio of less than 0.04 [2], and the current record device had an AAC of 0.19 [1]. One known advantage

This is an open access article under the terms of the [Creative Commons Attribution](https://creativecommons.org/licenses/by/4.0/) License, which permits use, distribution and reproduction in any medium, provided the original work is properly cited.

© 2025 The Author(s). Progress in Photovoltaics: Research and Applications published by John Wiley & Sons Ltd.

of Ag alloying in CIGS is that it lowers the melting temperature of the material and promotes crystal growth [3–5]. These benefits allowed Swiss Federal Laboratories for Materials Science and Technology (Empa) to reach 22.19% efficiency on a flexible substrate [6].

Previous studies have demonstrated that LS may both increase [7–10] and decrease [9, 11, 12] the open-circuit voltage (V_{oc}) of CIGS. LS effects have systematically been seen for CIGS deposited with co-evaporation [13], 2-step process (CIGSSe, sulphurisation and selenisation) [14, 15] and epitaxially grown [16]. An increase in open-circuit voltage has been associated with higher doping [1, 7, 11, 17] and sometimes accompanied with lower short-circuit current density (J_{sc}) due to a narrower space charge region [11–13, 18]. However, there is no consensus in the literature on the causes for the effects. Drift of alkali elements [12, 19], copper migration [20] and metastability of the amphoteric V_{Cu} - V_{Se} defect complex [21, 22] have all been suggested.

Alkali elements such as sodium and/or rubidium are commonly incorporated in CIGS processing as a precursor or using a post-deposition treatment (PDT). The treatments are typically observed to increase the p-type doping of the absorber [23]. Since the interstitial alkali defects are positively charged [24], it is probable that they move in the electric field in an operating device. Several pieces of evidence for alkali involvement in LS effects have been presented. An exponential relationship between the increase in doping and sodium concentration has been reported [19], and Matsuura et al. [12] showed that hot-light-soaking (HLS) only improved the V_{oc} for NaF treated cells and not for untreated devices. Furthermore, they saw that the Na and K concentrations increased near the front not only for HLS treated cells but also for forward biased devices [12]. A similar change in alkali profiles was seen by Carron et al. [17].

The V_{Cu} - V_{Se} defect complex as a model for metastability effects in CIGS was first proposed by Lany and Zunger [21, 22] who suggested that it can be converted from a donor to an acceptor by capture of an electron. The reverse transition is then inhibited by an energy barrier and the demand to capture two holes (compared to just one electron in the other direction). Since the proposed process is thermally activated the recovery can be accelerated with annealing. While the theory is able to explain the main behaviours during LS, and indications that the V_{Cu} - V_{Se} complex is present in ACIGS have been reported [11], it is not accepted as the sole explanation. The strongest counter argument is that the formation energy of the complex is too high, so the concentration must be insufficient to explain the magnitude of the observed effect [25].

An important parameter to keep in mind when discussing LS is the temperature of the devices, as they inevitably heat up due to light exposure. A majority of previous studies used HLS at temperatures above ambient in standard LS. Carron et al. [17] observed that the V_{oc} increase was more persistent for higher temperature during LS (80°C–120°C). Jahandardoost et al. [9] demonstrated complex dependencies on the temperature (65°C–85°C), buffer layer (ZnO vs. CdS), and configuration of the device during LS (short circuit or open circuit). Hence, also, the combined effects of light and heat on the defect distributions

in the contacts and at the absorber/contact interfaces have to be taken into account.

The incorporation of silver in CIGS adds a new dimension to the complex LS phenomena. A recent study from our group revealed that for ACIGS devices with high Ga content and AAC > 0.5 a reduction in net doping concentration and V_{oc} is observed after LS [26]. While Ferguson et al. light soaked ACIGS [11], their focus was ACIGS devices produced with varying Se supply to explore the role of the V_{Cu} - V_{Se} complex. The authors concluded that these complexes are active during LS in the Ag-alloyed absorbers.

This study is a comprehensive comparison between LS effects in highly efficient CIGS and ACIGS solar cells using photoluminescence (PL), current density–voltage (JV), external quantum efficiency (EQE), and capacitance–voltage (CV) measurements. The compositions ranged from $[I]/[III] \equiv ([Cu]+[Ag])/([In]+[Ga])$ of 0.84 to 0.93, $GGI \equiv [Ga]/([Ga]+[In])$ from 0.28 to 0.41, and the ACIGS samples had AAC values from 0.17 to 0.19. It is within these composition ranges that high efficiency of CIGS and ACIGS devices usually is found.

2 | Methods

In this section, the overall workflow of the light-soaking and characterisation is explained, as illustrated in the schematic in Figure 1.

2.1 | Sample Preparation and Initial Characterisation

From an initial batch of devices produced around the same time as the record device [1], a selection of 10 cells was made based on their electrical parameters and compositions. All devices had a stack of soda-lime glass (SLG)/Mo/(A)CIGS/CdS/i-ZnO/ZnO:Al, and all absorber layers were about 2 μm thick, grown with a modified three-stage co-evaporation process. A full description of the processing is given in Section 5. Before the initial JV measurements, all samples were in a dark (relaxed) state induced by long-term dark storage, but they had all been characterised shortly after being finalised. A summary of the measured electrical parameters and compositions is presented in Table 1. The efficiencies, η , ranged from 17.2% to 21.0%, and the AAC for the silver alloyed cells ranged from 0.14 to 0.19. All devices were postdeposition treated with RbF. Four out of 10 samples had MgF_2 anti-reflective coating (ARC), but this was deemed unimportant for the relative changes since Carron et al. [17] demonstrated no influence of ARC on the HLS effects. For PL measurements, a fragment of the full sample close to the selected cell was cut out and etched with acetic acid to remove the conducting transparent conductive oxide (TCO) layers: i-ZnO and ZnO:Al. This was needed to avoid lateral movement of charge carriers which would reduce the PL signal, as the carriers would be lost in the front contact.

2.2 | Electrical Characterisation

The selected cells underwent further electrical characterisation with EQE measurements. From the EQE data, a short-circuit current was calculated using the AM1.5 spectrum and

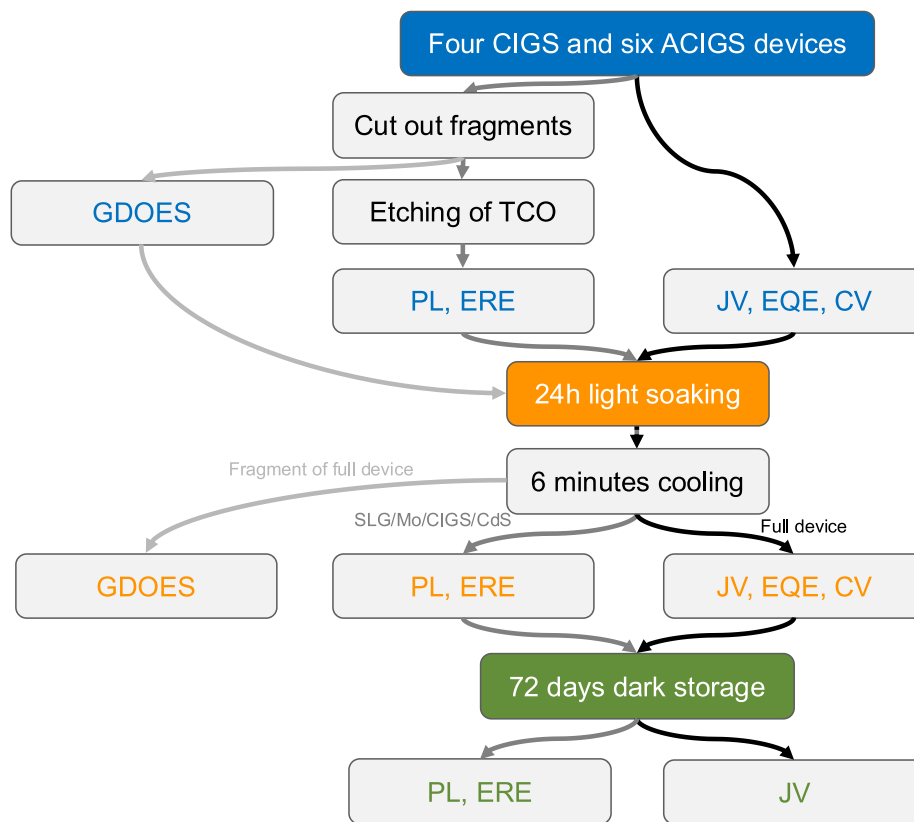


FIGURE 1 | Schematics of the workflow used in this study.

TABLE 1 | Electrical parameters and composition for selected devices before LS. [I]/[III], GGI and AAC ratios were all quantified with X-ray fluorescence measurements, with a sample with known composition as reference.

Sample	V_{oc} [mV]	J_{sc} [mA/cm ²]	FF [%]	η [%]	[I]/[III]	GGI	AAC
1	750	35.0	73.3	19.3 (1.03)	0.88	0.38	0.00
2	714	35.1	68.7	17.2 (1.03)	0.93	0.40	0.00
3	745	35.0	74.6	19.5 (1.07)	0.87	0.40	0.00
4	722	35.0	68.9	17.4 (1.05)	0.92	0.40	0.00
5 ARC	700	38.1	74.0	19.8 (1.09)	0.86	0.39	0.17
6	734	35.6	72.8	19.0 (1.04)	0.84	0.34	0.19
7	738	35.5	72.8	19.1 (1.08)	0.85	0.35	0.19
8 ARC	702	38.4	75.8	20.4 (1.00)	0.84	0.28	0.19
9 ARC	742	37.0	76.4	21.0 (0.93)	0.86	0.28	0.19
10 ARC	689	38.4	74.2	19.6 (0.99)	0.84	0.28	0.19
WR (24 h LS) ARC	767	38.3	80.5	23.6	0.84	0.28	0.19

Note: The J_{sc} values (active area) are extracted from EQE measurements and the η values were corrected by the factor J_{sc}^{EQE}/J_{sc}^{JV} (given in parenthesis). Corresponding values for the world record (WR) device (after 24 h LS) are also given for comparison [1].

a correction factor, J_{sc}^{EQE}/J_{sc}^{JV} , was determined. The J_{sc} and η values from JV measurements were multiplied by this obtained factor, ranging from 0.93 to 1.09. Subsequently, CV characterisation in dark at room temperature was performed on all cells. A detailed description of the characterisation is done in Section 5.

2.3 | Light-Soaking and Post-Light-Soaking Characterisation

Directly after the initial JV, EQE and CV analyses, all 10 devices were light-soaked in open circuit configuration for 24 h in ambient atmosphere with the spectral irradiance

corresponding to one-third of the AM15 spectrum. Since no active cooling was in place, the devices' temperatures reached approximately 50°C, and they were allowed to cool for 6 min at room temperature before post-LS characterisation. Measurements of JV, EQE and CV were conducted in the same manner as before LS, in the listed order. Glow-discharge optical emission spectroscopy (GDOES) measurements were also performed on the full-stack solar cells before and after LS. The absorber compositions from X-ray fluorescence (XRF) data were used to quantify GGI, [I]/[III] and AAC ratios in the absorber region. All samples' GGI, Se and AAC profiles are given in Figures S1 and S2.

To further explore the LS effects, one CIGS (Sample 3) and one ACIGS (Sample 5) device were monitored for 48 h during LS. JV measurements were conducted after 1, 2, 4, 6, 24 and 48 h. When the post-LS characterisation was completed, all devices were kept in dry, dark storage (DS) for 72 days. After this, JV measurements were repeated to explore the duration and reversibility of the LS effects.

2.4 | Photoluminescence Measurements

The stacks of SLG/Mo/(A)CIGS/CdS were used for external radiative efficiency (ERE) measurements at three different positions under one-sun excitation. A more detailed explanation of the procedure is given in Section 5.1, and the underlying theory is presented in Section 2.4.1. The CdS layer was not etched away because it protects the (A)CIGS surface from degradation, but possible changes in the CdS/(A)CIGS interface are also included in the further analysis [27]. After the initial PL measurements, all pieces were subjected to LS in the same manner as the devices and left to cool for 6 min before the measurements were repeated.

In analogy with the JV characterisation of devices 3 and 5, the ERE measurements were also conducted after 1, 2, 4, 6, 24 and 48 h of LS for the corresponding sample pieces. Furthermore, the ERE measurements of all absorber stacks were repeated after 72 days of DS.

2.4.1 | External Radiative Emission Measurements

The ERE is defined as the ratio between the number of photons emitted to the number of photons generated under illumination. The PL measurements in this paper are not absolute, but the ERE is measured using an integrating sphere to quantify the ratio between emitted and absorbed photons. This is same as the fraction of radiative recombination compared to the total recombination. The measured ERE can be used to calculate the quasi-Fermi level splitting, ΔE_F , of the absorber through the equation

$$\Delta E_F = qV_{oc}^{SQ} + kT \ln ERE, \quad (1)$$

where q is the elemental charge, k the Boltzmann constant and V_{oc}^{SQ} is the open-circuit voltage in the Shockley–Queisser limit [28]. Ideally, the quasi-Fermi level splitting of the absorber is the maximum achievable open-circuit voltage of the corresponding full solar cell. The V_{oc}^{SQ} depends on the bandgap, which can

be extracted from the inflection point of the EQE spectrum [29]. However, this does not take radiative losses due to tail states into account since subbandgap absorption in the Shockley–Queisser limit is zero. More tail states shift the PL maximum towards lower energies [30, 31]. If the PL peak energy is used as bandgap in the Shockley–Queisser theory, a V_{oc}^{rad} is obtained, where losses due to tail states and bandgap fluctuations are somewhat accounted for [28]. Depending on how broad the distribution of alternative bandgaps coming from tail states is, using V_{oc}^{rad} instead of V_{oc}^{SQ} may underestimate (for a broad distribution) or overestimate (for a very narrow distribution) the calculated ΔE_F [31]. Furthermore, the ΔE_F divided by q should be equal to the measured V_{oc} provided interfacial losses are negligible [28]. One possible source of such interfacial losses is substantial band misalignment between the absorber, buffer and contact layers [28].

2.4.2 | Tail States

While an ideal semiconductor has a sharp onset of absorption at a wavelength corresponding to the bandgap, this is not the case in actual materials and especially in polycrystalline, heavily defected materials such as CIGS. States near the band edges makes absorption decay exponentially, with the rate characterised by the Urbach energy, E_{urb} , so that below the bandgap the absorption coefficient, α , and the photon energy, E , are related via [32]

$$\frac{d \ln \alpha(E)}{dE} = \frac{1}{E_{urb}}. \quad (2)$$

Local bandgap differences in CIGS can be caused by local composition fluctuations (in terms of GGI and [I]/[III] ratios), disorder and strain (lattice distortion) [33]. Electrostatic potential fluctuations due to charged impurities may also influence the absorption coefficient [34, 35]. Since the PL emission flux $\Phi_{PL}(E)$ is given by [28, 36]

$$\Phi_{PL}(E) = A(E)\Phi_{BB}(E)e^{\frac{\Delta E_F}{kT}} \approx A(E)\frac{E^2}{4\pi^2\hbar^3c^2}e^{-(E-\Delta E_F)/kT}, \quad (3)$$

where E is the photon energy and Φ_{BB} is the black body radiation flux, the effective absorption $A(E)$ can be extracted from an absolute PL measurement [28] as

$$A(E) \approx 4\pi^2\hbar^3c^2 \frac{\Phi_{PL}(E)}{E^2e^{-(E-\Delta E_F)/kT}}. \quad (4)$$

In the low absorption regime, $\ln(1-A) \approx -A$. Considering that the absorption coefficient $\alpha = -\ln(1-A)/x$, where x is the thickness of the absorber, it can be rewritten as

$$\alpha(E) \approx \frac{A(E)}{x}. \quad (5)$$

Since $A(E)$ can be extracted from a PL measurement, $\alpha(E)$ can also be derived using Equation (5). Even if the PL measurement is not absolute but proportional to the absolute spectrum, the Urbach energy can be obtained from

$$\frac{1}{E_{urb}} = \frac{d}{dE} \ln \frac{\Phi_{PL}(E)}{E^2e^{-E/kT}}, \quad (6)$$

because x and $e^{\Delta E_F/kT}$ are independent of the photon energy. It should be noted that extraction of Urbach energies from EQE data is also possible, provided enough data points in the sub-bandgap region can be collected.

In this paper, PL spectra recorded during ERE measurements were used to extract the Urbach energies of different samples. From a plot of $\ln \frac{\Phi_{PL}}{E^2 e^{-E/kT}}$ vs. E , based on Equation (6), a linear fit of the sub-bandgap absorption was made and the inverse of the slope was extracted as the Urbach energy. Fifty data points starting either 40 or 30 nm (range is here given in nm as the spectra are acquired with constant wavelength steps) below the PL maximum was used for the fit, depending on the location of the linear region.

3 | Results and Discussion

In Table 2, electrical parameters extracted from JV measurements for the cells before LS, after LS and after DS are presented. EQE spectra before and after LS can be found in Figures S3 and S4. For clarity, the open-circuit voltages are also illustrated in Figure 2a. A systematic difference between CIGS (Samples 1–4) and ACIGS (Samples 5–10) is evident. The CIGS samples' V_{oc} decreased after LS (by 5–31 mV), while the V_{oc} of all ACIGS samples increased substantially (by 18–73 mV). No significant changes in J_{sc} were seen. The fill factor (FF) increased for ACIGS devices and decreased for all CIGS devices except Sample 4. As a consequence, the power conversion efficiency η of the ACIGS devices and the CIGS Sample 4 improved while dropping for the rest of the CIGS cells. The corresponding dependence with respect to composition ratios can be found in Figures S5–S7. Besides the clear divide with Ag alloying, no other correlations have been found. We note that the CIGS and ACIGS are also grouped by the [I]/[III] and GGI ratio, but we still speculate that the difference can be attributed to silver

incorporation. For example, CIGS Sample 1 and ACIGS Sample 5 behave differently even though they are close in both [I]/[III] (0.88 vs. 0.86) and GGI (0.38 vs. 0.39) ratios. The 2.5 months of DS partially reversed the change in V_{oc} , but at a much slower rate, except for Sample 3 that lost even more voltage after DS.

3.1 | External Radiative Efficiency

The ERE is expected to follow the V_{oc} if no drastic change occurs at the ZnO/CdS interface, and this is confirmed in Figure 2a,b. The ACIGS Sample 8 reached ERE = 2.1% after LS, to the best of our knowledge the highest ERE ever measured for a chalcopyrite absorber. In order to apply Equation (1), V_{oc}^{SQ} has to be calculated and a bandgap is therefore needed. The bandgaps were extracted from the EQE spectra using the maximum of the first derivative (also known as the inflection point method), as suggested by Rau et al. [29, 37]. All bandgaps and EQE data before LS (no significant change was seen with LS) can be found in Table S1.

Before LS, Sample 8 had a bandgap of 1.12 eV, which gives $V_{oc}^{SQ} = 862$ mV and $\Delta E_F/q = 752$ mV, higher than the electrically measured 702 mV. After LS, the bandgap is unchanged and with an increased ERE = 2.1% the same calculation gives $\Delta E_F/q = 765$ mV. This value matches the measured 765 mV, which is unlikely as the quasi-Fermi level splitting should in practice be larger than the measured V_{oc} (note that this situation is true also for the 1.6% ERE of the record absorber in [1]). The additional loss from radiative recombination via tail states typically amounts to about 10–20 mV [31], and this is not accounted for in the measured quasi-Fermi level splitting. Using the PL peak position as the bandgap yields a V_{oc}^{rad} of 853 mV and a $V_{oc}^{rad} - kT/q \ln ERE = 756$ mV, even lower than the measured open-circuit voltage. This artifact may be due to miscalibration of the setup (so that the ERE is actually higher than 2.1%), or the sample fragment the ERE is measured on is not representative for the actual device.

TABLE 2 | Electrical parameters of the devices before LS, after 24 h LS and after 72 days of DS.

Sample	V_{oc} [mV]			J_{sc} [mA/cm ²]			FF [%]			η [%]		
	Initial	24 h LS	DS	Initial	24 h LS	DS	Initial	24 h LS	DS	Initial	24 h LS	DS
CIGS												
1	750	719	735	35.0	35.2	35.1	73.3	64.9	70.2	19.3 (1.03)	16.4 (1.02)	18.1
2	714	699	711	35.1	34.6	34.0	68.7	61.5	68.2	17.2 (1.03)	14.9 (0.99)	16.5
3	745	740	736	35.0	34.7	33.7	74.6	73.5	74.0	19.5 (1.07)	18.9 (1.05)	18.3
4	722	712	727	35.0	34.9	35.6	68.9	70.7	71.1	17.4 (1.05)	17.6 (1.02)	18.4
ACIGS												
5 ARC	700	762	734	38.1	38.0	35.9	74.0	75.3	74.1	19.8 (1.09)	21.8 (1.03)	19.5
6	734	752	749	35.6	35.7	34.0	72.8	77.2	73.1	19.0 (1.04)	20.7 (0.98)	18.6
7	738	757	749	35.5	35.4	32.4	72.8	74.2	72.8	19.1 (1.08)	19.9 (1.05)	17.7
8 ARC	702	765	732	38.4	38.1	37.4	75.8	76.9	76.2	20.4 (1.00)	22.4 (1.00)	20.9
9 ARC	742	769	750	37.0	36.5	36.6	76.4	77.8	76.5	21.0 (0.93)	21.8 (0.94)	21.0
10 ARC	689	762	712	38.4	38.4	40.1	74.2	75.4	74.6	19.6 (0.99)	22.1 (0.94)	21.3

Note: The J_{sc} values were extracted from EQE measurements before LS and after 24 h of LS (not for DS), and the η values were corrected by the factor J_{sc}^{EQE}/J_{sc}^{JV} . The correction factor is given in parenthesis after the η values.

Discrepancies between quasi-Fermi level splitting and the measured voltage ($\Delta E_F/q < V_{oc}$) have previously been reported to depend on different excitation wavelengths and connected to the graded bandgap of the absorber, but no convincing explanation has been provided yet [31]. Especially for the CIGS devices in this study, extraction of an effective bandgap by the inflection point method was ambiguous because of the low-energy bumps in the EQE spectra, as illustrated in Figure 3a. This bump is likely due to the GGI gradient, also exemplified in Figure 3b by the measured GDOES profiles. The very steep decrease in GGI

towards the surface indicates the presence of a thin low band-gap surface phase. In contrast, the ACIGS samples have more monotonic GGI profiles. An effort was made to replicate the EQE bump using SCAPS-1D for a model bandgap profile and the simulation results indeed showed a good qualitative agreement, as illustrated in Figure S8.

Using the inflection point from the bump and above the bump from the CIGS devices' EQE spectra, two sets of bandgaps and corresponding V_{oc}^{SQ} values could be determined and used for the

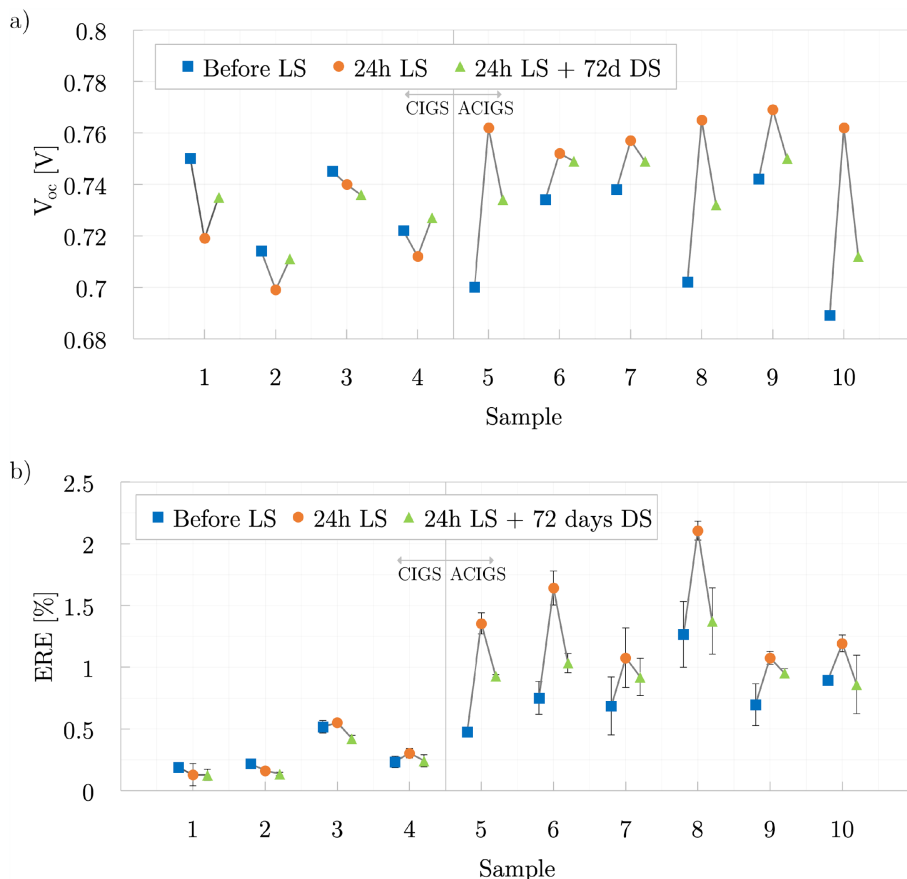


FIGURE 2 | V_{oc} (a) and ERE (b) changes for all samples (1–4 CIGS, 5–10 ACIGS) before light-soaking, after 24 h of light-soaking and after subsequent 72 days of dark storage. The ERE values are average values of three different measurement points (two for Sample 5 after LS) with error bars corresponding to the standard deviation.

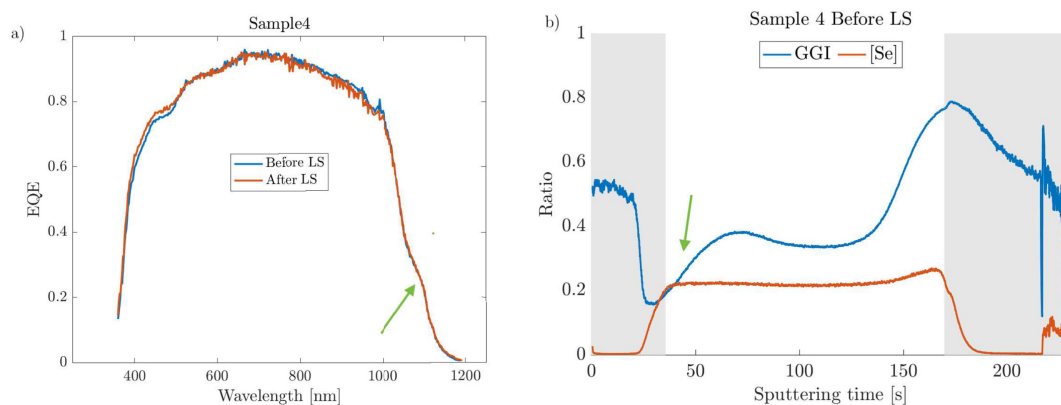


FIGURE 3 | The EQE spectra for Sample 4 (a) and the corresponding GGI ratio from GDOES measurements (b). The green arrow indicates the low-energy bump around 1100 nm in the EQE spectrum and the steep GGI decrease at the front.

quasi-Fermi level splitting calculations. The difference between these results is illustrated in Figure 4 (before LS in Figure 4a, after LS in Figure 4b and after DS in Figure 4c). It is probable that an effective bandgap, that would be more appropriate to use

in Equation (1), is somewhere in between the two extremes. For the ACIGS devices, it is worth mentioning that Samples 5, 8 and 10 have a larger difference between the measured V_{oc} and that estimated from the ERE before LS. The measured V_{oc} , however,

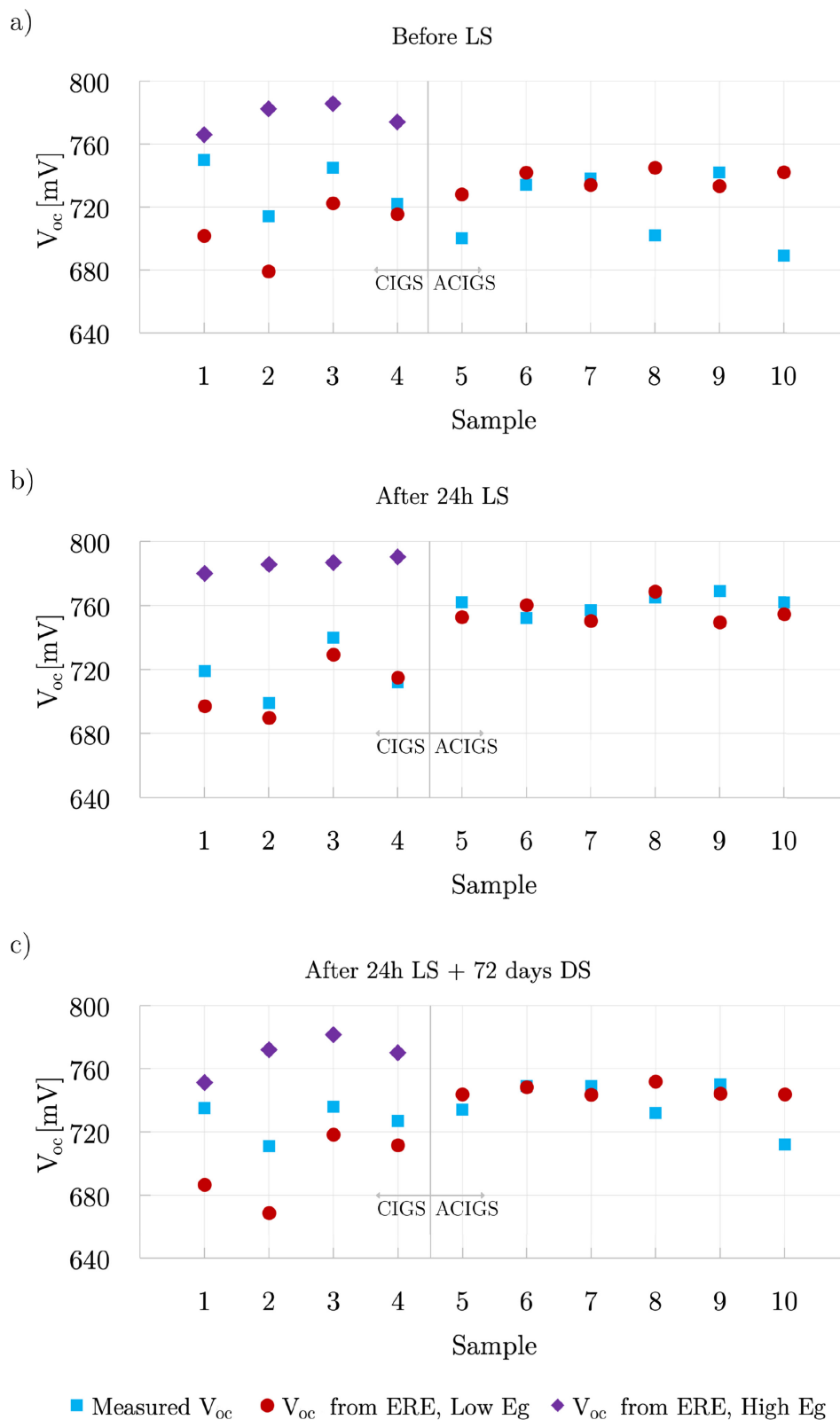


FIGURE 4 | The measured V_{oc} and the V_{oc} calculated from ERE using bandgaps extracted from EQE measurements. For the CIGS devices two different inflection points, that is, bandgaps, could be determined, and hence, two V_{oc} from ERE are plotted. No EQE bump was observed for ACIGS devices; hence, the bandgap is unambiguously determined.

almost matches the estimated values after LS, but the difference increases again after DS.

3.2 | Dynamics of the Effect

The discussed difference between LS behaviour of ACIGS and CIGS is clearly illustrated by the evaluation of V_{oc} and ERE during LS in Figure 5a,b, respectively. The ACIGS Sample 5 increased in both ERE (from 0.50% to 1.42%) and V_{oc} (from 706 to 762 mV), saturating after 24 h of LS, in analogy with the behaviour of the record cell [1]. The main part of the improvement takes place in the first 6 h, and it could be even quicker at higher temperatures or under a full sun illumination LS. In contrast, the CIGS Sample 3 shows only minor fluctuations in V_{oc} (between 743 and 738 mV) and ERE (between 0.32% and 0.53%). We acknowledge that Sample 3 behaved differently compared to the other CIGS cells as it was the only one that did not recover after 72 days in dark, as seen in Figure 2a. This may be connected to the increased handling of the sample during LS. A full set of JV curves recorded for different LS times are shown in Figure S9.

3.3 | Apparent Doping Density

An increased quasi-Fermi level splitting can stem from two sources: (i) the hole quasi-Fermi level moving closer to the valence band or (ii) the electron quasi-Fermi level moving closer to the conduction band (if the bandgap is constant). In a p-type semiconductor like CIGS under low excitation the former is a consequence of higher doping, while the latter is caused by longer electron lifetimes. For the devices in this study, the apparent doping levels and depletion region widths were extracted from CV measurements. The results summarised in Table 3 reveal that the increased quasi-Fermi level splitting and open-circuit voltage observed for the ACIGS solar cells could be attributed to higher doping.

From the data in Figure 6, it is clear that the depletion width of CIGS Samples 1–4 was already very narrow before LS (0.19–0.30 μm). Therefore, an order of magnitude change in apparent doping from the low 10^{16} cm^{-3} to values closer to 10^{17} cm^{-3} did not have a large absolute effect on the depletion width. The apparent doping of the ACIGS Samples 5–10 was however much smaller from the beginning, in the order 10^{15} cm^{-3} , so the increase to around 10^{16} cm^{-3} shrank the depletion region significantly. The narrowing of the depletion width does not adversely affect the carrier collection as the short-circuit current remains

unaffected by LS. This behaviour indicates that the samples have long diffusion lengths and that the effective lifetimes are stable, in contrast to the results by Heise et al. where the minority carrier lifetime decreased [18]. Nevertheless, we cannot exclude a reduction that would not be visible in the EQE spectrum. A reduced lifetime would counter the hole quasi-Fermi level shift, possibly reducing the V_{oc} .

Incorporation of alkali elements in CIGS is commonly suggested to be beneficial by increasing the p-type doping (Na) and/or by defect passivation at grain boundaries and absorber surfaces (K, Rb, Cs) [23]. Considering the increased solubility of alkalis upon Ag alloying [38], the different behaviours of CIGS vs. ACIGS under LS may be connected to alkali. However, our GDOES measurements for Na and Rb showed no significant difference neither between ACIGS and CIGS nor before and after LS, as can be seen in Figures S10 and S11. We estimate (based on contact with the system manufacturer) the resolution of the GDOES used here to be in the order 10^{17} cm^{-3} for Na and 10^{18} cm^{-3} for Rb. Both these values are larger than the apparent doping concentration, and therefore, even if the change in doping is dictated by a long-distance drift of alkalis, the effect is beyond the resolution of GDOES. Moreover, small local

TABLE 3 | Apparent doping density and the corresponding depletion region widths before and after 24 h of LS.

Sample	Apparent doping [cm^{-3}]		Depletion width [μm]	
	Before LS	After LS	Before LS	After LS
1	$1.0 \cdot 10^{16}$	$5.6 \cdot 10^{16}$	0.21	0.08
2	$1.1 \cdot 10^{16}$	$2.6 \cdot 10^{16}$	0.20	0.11
3	$4.8 \cdot 10^{15}$	$3.0 \cdot 10^{17}$	0.30	0.05
4	$1.1 \cdot 10^{16}$	$1.3 \cdot 10^{17}$	0.19	0.06
5	$6.7 \cdot 10^{15}$	$2.3 \cdot 10^{16}$	0.57	0.20
6	$3.6 \cdot 10^{14}$	$6.2 \cdot 10^{16}$	1.05	0.10
7	$5.3 \cdot 10^{14}$	$2.2 \cdot 10^{16}$	1.22	0.18
8	$4.8 \cdot 10^{14}$	$1.4 \cdot 10^{16}$	1.36	0.25
9	$4.3 \cdot 10^{14}$	$1.6 \cdot 10^{16}$	1.26	0.22
10	$1.2 \cdot 10^{15}$	$9.6 \cdot 10^{16}$	1.11	0.30

Note: The values are averages of two CV measurements with different sweeping directions.

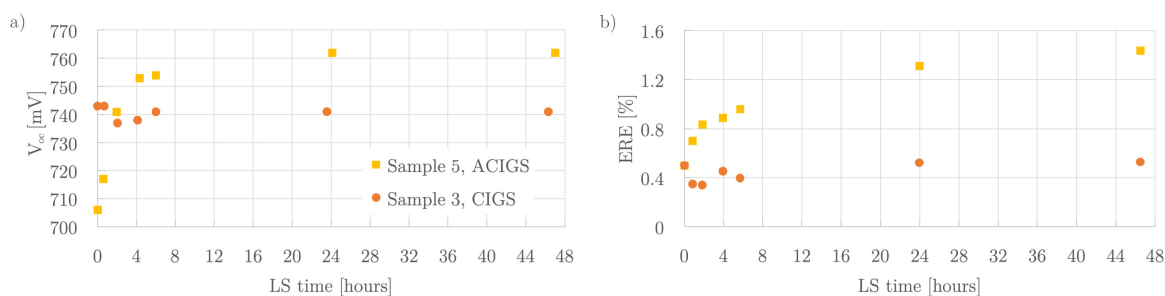


FIGURE 5 | Open-circuit voltage and ERE of Samples 5 and 3 at different LS times. Note that the initial ERE of both devices is the same.

(or lateral) movement are principally invisible in the compositional depth profiling and hence cannot be excluded. These movements of charged alkali species may still induce electrical polarization after biasing or LS in the open-circuit configuration. The resulting polarization might thus be yet another contributor to the complex LS effects. Furthermore, secondary ion mass spectroscopy, as used by Matsuura et al. [12] and Carron et al. [17], might be able to detect long range re-distribution, because the technique is more sensitive. In fact, these earlier studies both showed an increased alkali concentration at the buffer/absorber interface after LS.

3.4 | Tail States

While the increased apparent doping density is expected to give a higher open-circuit voltage, an increase in Urbach energy is expected to decrease it. The Urbach energies extracted from PL measurements are presented in Figure 7. For some samples, the spread of the data points is very large, but there is an overall trend of higher Urbach energy after LS, and the values are within the range of what has previously been reported for CIGS [39]. The trend is furthermore reflected in a redshift of the PL peak after LS, as shown in Figure 8, and by a tail shift of the low energy part of the EQE spectrum, as depicted in Figure S12. Hence, an increased contribution of tail states after LS is confirmed, in contrast to the observations by Carron et al. [17]. Using the equation $\Delta V_{oc}^{rad} = kT/q \ln(1 - E_{urb}/kT)$ [40], the average V_{oc}^{rad} reduction for the CIGS samples due to the increased tail states amounts to about 6 mV, which could partly explain the V_{oc} reduction seen for the CIGS samples. The reduction caused by both the extra radiative and nonradiative recombination via tail states when E_{urb} changes from 12 to 14 mV is estimated to be about 9 mV based on the calculations by Wolter et al. [39]. Hence, the increased Urbach energy alone cannot explain the voltage reduction seen for the CIGS devices.

An increased presence of tail states can originate from more bandgap variations and electrostatic potential fluctuations [30]. These can be caused by local variations of compositions, disorder, lattice strains or charged point defects [30]. When the $V_{Cu}-V_{Se}$ complex transforms from a shallow donor to a shallow acceptor, it results in a defect energy level close to the conduction band [22]. The increase in active tail states could therefore be related to direct optical transitions to that in-gap defect state becoming more frequent as the concentration of the acceptor complexes is increased after LS.

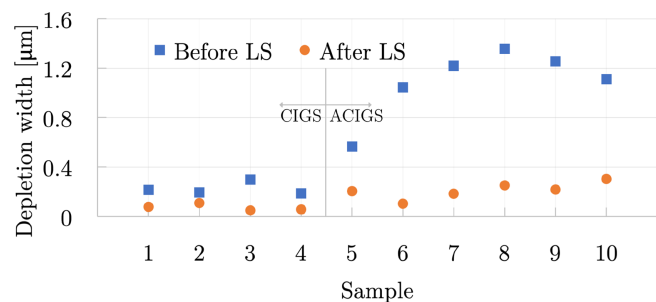


FIGURE 6 | Depletion widths for all samples (1–4 CIGS, 5–10 ACIGS) before and after 24 h of light-soaking.

3.5 | Discussion

In this work, we analysed a combination of ACIGS and CIGS devices and observed that LS was detrimental for the CIGS and beneficial for the ACIGS cells. The main proposed explanations for LS effects are metastable defects, alkali redistribution and copper migration, but a mixture of all these effects is also possible. Carron et al. suggested that the initial response is connected to the $V_{Cu}-V_{Se}$ complex while the later and persisted change is attributed to alkali. As far as we know, no counter evidence has ever been given for Cu migration, so this may also be related to the LS effect, in a similar way as alkali migration. However, in this study, no systematic changes in GDOES profiles for AAC and [I]/[III] were seen after LS. All of these phenomena may act differently in ACIGS as compared to CIGS, and this study does not exclude any of them.

Several previous studies [7–10] have shown that CIGS cells improve under light exposure. Hence, our samples are atypical, and thus, we do not claim that LS is a general issue for CIGS. Rather, our findings highlight the complexity of the LS effects, and that for some devices, increased recombination either in the bulk or interface may cause a decreased open-circuit voltage. While the main difference between the cells in this study was the silver content, they were slightly different in both GGI profile and [I]/[III] composition ratio, and future studies should aim to keep these constant. In addition, LS studies where the initial state of the devices is not merely relaxed (dark) but newly produced would also be desirable.

As shown by Jahandardoost et al. [9] and Nikolaeva et al. [41], the buffer layer interface may also be of importance. Silver incorporation in CIGS shifts the band edges [42], which potentially could be

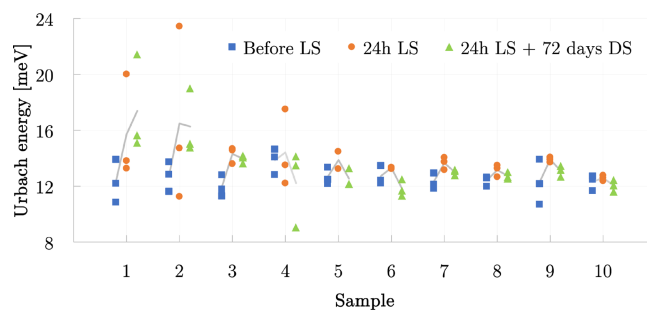


FIGURE 7 | Urbach energies extracted from PL spectra from three different places before LS, after 24 h of LS and after subsequent DS. The lines show how the mean of the three data points evolves.

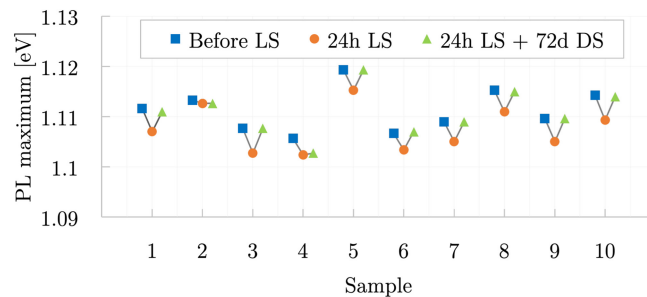


FIGURE 8 | Average PL peak position (1–4 CIGS, 5–10 ACIGS) before LS, after 24 h of LS and after LS and DS.

connected to the different behaviours of CIGS and ACIGS. It is also known that the CdS layer undergoes photodoping [43], although this is believed to happen within minutes [44]. Furthermore, Nikolaeva et al. [41] found that the amplitude of electrostatic fluctuations decreased after LS, which is in contrast to the increased Urbach energy seen in this study. The reason for the more active tail states is beyond the scope of this study but appears connected to the higher doping.

Lastly, as pointed out by the record device [1], light-soaking is currently needed to maximise the efficiency. Since the devices in this study are closely related to the record CIGS solar cell, they are highly relevant to understand why this is the case. In modules, prediction of the working point of the cells is important, and these metastable fluctuations can cause problems as diurnal and seasonal irradiation variations will cause efficiency fluctuations. However, since the relaxation to the low efficiency state of ACIGS takes much longer than a day, diurnal variations may not be problematic. Furthermore, bottom cells in tandem devices will only be exposed to red illumination, which may not induce the ACIGS high efficiency doping state. This needs to be addressed by future studies.

4 | Conclusion

In this study, we used 10 highly efficient CIGS and ACIGS solar cells and analysed their response to 24 h of light-soaking at around 50°C. The devices were produced using the same deposition system as the record device but with slightly varied compositions. We found a systematic difference where the ACIGS devices' V_{oc} increased and the CIGS devices' V_{oc} decreased. The improvement for ACIGS was quick during the first 12 h and saturated after 24 h. All devices reached a metastable state after LS and subsequent 72 days of dark storage brought them back towards their initial state. The apparent doping increased for all devices, but the CIGS doping in the relaxed (dark) state was 10^{16} cm^{-3} compared to 10^{15} cm^{-3} for ACIGS. Therefore, an order of magnitude higher values after LS caused greater depletion width changes for the ACIGS devices. In general, the open-circuit voltage change was accompanied with a corresponding change in ERE, i.e. decreased nonradiative recombination, for the ACIGS devices, but the absolute open-circuit voltage change did not always match the estimations based on the ERE. Nevertheless, a record ERE of 2.1% was measured on an ACIGS absorber, leading to an efficiency of 22.4%. In all devices, the metastable state after light-soaking had more active tail states, deduced from PL measurements. While alkali involvement cannot be excluded, no difference in the depth-profiles of rubidium and/or sodium before and after light-soaking was seen. Whatever the mechanism for the CIGS LS effect is, this study indicates that it may be modified with silver alloying.

5 | Experimental

The solar cells discussed in this paper have the full stack sequence: SLG/Mo/NaF-precursor/(A)CIGS/RbF-PDT/CdS/i-ZnO/ZnO:Al/(MgF₂). The 290-nm-thick Mo back contact was DC magnetron sputtered and then coated with a thermally evaporated 10-nm-thick NaF precursor layer. On top of this, the (A)CIGS absorber layer was grown with a modified three-stage co-evaporation

process so that the absorbers were 1.9–2.2 μm thick. The maximum substrate temperature reached during the deposition was about 530°C. After the absorber deposition, a 3 to 5 nm RbF layer was applied as PDT at 330°C–350°C, without additional Se supply and without breaking the vacuum. Thereafter, a CdS buffer layer of around 25–30 nm was grown via chemical bath deposition at 60°C. Lastly, a 30-nm-thick i-ZnO and 230-nm-thick ZnO:Al layer were both deposited with RF- and DC-sputtering, respectively. The areas of the solar cells were between 0.453 and 1.13 cm^2 .

GDOES measurements were done with a Spectrumba Analytik GDA 750HR system (measured area about 3 mm^2). Quantification of the absorber elements was done with corresponding XRF data. Limits for the absorber region were set to the depths where 90% of the selenium signal's local maximum (in the front and back) was reached. All JV measurements were done at 25°C in a home-built setup with a halogen lamp and a Si reference cell to calibrate for one sun illumination. EQE measurements were done in a home-built setup with a xenon lamp calibrated using InGaAs and Si photodetectors. An Agilent 4284 A Precision LCR Meter and a frequency of 60 kHz was used for the CV measurements. An initial zero bias measurement was performed to exclude hysteresis effects, and thereafter, forward and reverse sweeps from -0.5 to 0.3 V were carried out. To calculate the apparent doping and depletion region width, a material permittivity of 10 was assumed [45].

5.1 | Photoluminescence and ERE Measurements

For PL and ERE measurements, a piece of the full sample close to the selected cell was cut out and etched to a stack of SLG/Mo/(A)CIGS/CdS with acetic acid prior to LS. The ERE values were obtained under excitation of a 520 nm continuous wave laser, calibrated to one sun photon flux, incorporated in a FSL1000 PL spectrophotometer from Edinburgh instruments. An integrating sphere and a nitrogen cooled photomultiplier tube were used for detection. The sample emission (E) and scattering in the laser wavelength region (S) were recorded, followed

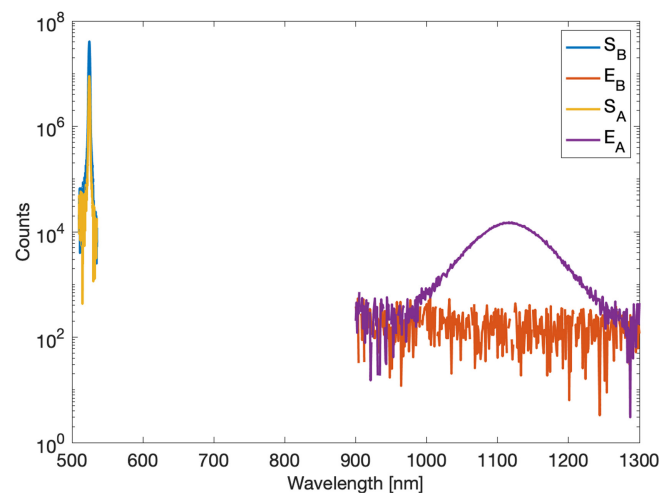


FIGURE 9 | Example of the four measurements used for the ERE calculation for Sample 8 after LS. The calculations according to Equation (7) yielded $\text{ERE} = 2.1\%$.

by measurements of the background using a BaSO₄ plug instead of the sample. After scaling the background to match that in the sample spectra, the signals were integrated and the ERE was calculated as

$$ERE = \frac{\int E_A d\lambda - \int E_B d\lambda}{\int S_B d\lambda - \int S_A d\lambda}, \quad (7)$$

where the subscript A is for the sample and B for the BaSO₄. An example of the four measurements for Sample 8 is presented in Figure 9. The PL peak and Urbach energies were extracted from the samples' emission spectra.

Author Contributions

Klara Kiselman and Jan Keller designed the light-soaking experiment. Klara Kiselman then performed the JV, EQE, PL and GDOES characterisation and corresponding data treatment. Patrick Pearson and Klara Kiselman did the CV measurements. Kostiantyn Sopiha and Jan Keller assisted in the analysis and interpretation of the results. Erik Wallin and Marika Edoff developed the (A)CIGS process. Marika Edoff supervised the work. Klara Kiselman wrote the paper with input from the co-authors. All authors reviewed the paper.

Acknowledgements

The authors acknowledge the financial support received from the Swedish Energy Agency through the project "The Solar Electricity Research Centre (SOLVE)", grant number 52693-1a and the project "Advanced optical concepts in ACIGS solar cells", project number 43523-2.

Conflicts of Interest

The authors declare no conflicts of interest.

Data Availability Statement

Data are available upon request.

References

1. J. Keller, K. Kiselman, O. Donzel-Gargand, et al., "High-Concentration Silver Alloying and Steep Back-Contact Gallium Grading Enabling Copper Indium Gallium Selenide Solar Cell With 23.6% Efficiency," *Nature Energy* 9 (2024): 467–478, Publisher: Nature Publishing Group, <https://www.nature.com/articles/s41560-024-01472-3>.
2. M. Nakamura, K. Yamaguchi, Y. Kimoto, Y. Yasaki, T. Kato, and H. Sugimoto, "Cd-Free Cu(In,Ga)(Se,S)₂ Thin-Film Solar Cell With Record Efficiency of 23.35%," *IEEE Journal of Photovoltaics* 9, no. 6 (2019): 1863–1867, Conference Name: IEEE Journal of Photovoltaics, <https://ieeexplore.ieee.org/document/8825469>.
3. G. M. Hanket, J. H. Boyle, and W. N. Shafarman, "Characterization and Device Performance of (AgCu)(InGa)Se₂ Absorber Layers," in *2009 34th IEEE Photovoltaic Specialists Conference (PVSC)*, (2009): 1240–001245, <https://ieeexplore.ieee.org/document/5411241>.
4. S. Soltanmohammad, H. M. Tong, T. J. Anderson, and W. N. Shafarman, "Reaction Rate Enhancement for Cu(In,Ga)Se₂ Absorber Materials Using Ag-Alloying," *IEEE Journal of Photovoltaics* 9, no. 3 (2019): 898–905 en, <https://ieeexplore.ieee.org/document/8651328/>.
5. L. Chen, J. Lee, and W. N. Shafarman, "The Comparison of (Ag,Cu)(In,Ga)Se₂ and Cu(In,Ga)Se₂ Thin Films Deposited by Three-Stage Coevaporation," *IEEE Journal of Photovoltaics* 4, no. 1 (2014): 447–451,

Conference Name: IEEE Journal of Photovoltaics, <https://ieeexplore.ieee.org/document/6600988>.

6. S. Nishiwaki, S.-C. Yang, M. Krause, A. N. Tiwari, and R. Carron, "Ag-Alloyed CIGS Solar Cells on Flexible Polymer Film With Record Efficiency of 22.2%," (2022).
7. M. Nardone, Y. Patikirige, K. E. Kweon, et al., "Quantifying Large Lattice Relaxations in Photovoltaic Devices," *Physical Review Applied* 13, no. 2 (2020): 24025, <https://link.aps.org/doi/10.1103/PhysRevApplied.13.024025>.
8. S. Ishizuka, N. Taguchi, J. Nishinaga, Y. Kamikawa, S. Tanaka, and H. Shibata, "Group III Elemental Composition Dependence of RbF Postdeposition Treatment Effects on Cu(In,Ga)Se₂ Thin Films and Solar Cells," *Journal of Physical Chemistry C* 122, no. 7 (2018): 3809–3817, Publisher: American Chemical Society, doi:10.1021/acs.jpcc.8b00079.
9. M. Jahandardoost, M. Nardone, T. M. Friedlmeier, C. Walkons, and S. Bansal, "Heat- and Light-Soaking Behavior of RbF-Treated Cu(In,Ga)Se₂ Solar Cells With Two Different Buffer Layers," *Journal of Materials Research* 37, no. 2 (2022): 436–444, <https://link.springer.com/10.1557/s43578-021-00472-3>.
10. C. Walkons, M. Jahandardoost, T. M. Friedlmeier, et al., "Behavior of Na and RbF-Treated CdS/Cu(In,Ga)Se₂ Solar Cells With Stress Testing Under Heat, Light, and Junction Bias," *Physica Status Solidi (RRL) - Rapid Research Letters* 15, no. 2 (2021): 2000530 en, <https://onlinelibrary.wiley.com/doi/10.1002/pssr.202000530>.
11. A. J. Ferguson, R. Farshchi, P. K. Paul, et al., "Defect-Mediated Metastability and Carrier Lifetimes in Polycrystalline (Ag,Cu)(In,Ga)Se₂ Absorber Materials," *Journal of Applied Physics* 127, no. 21 (2020): 215702, doi:10.1063/1.5134502.
12. J. Matsuura, I. Khatri, T.-Y. Lin, M. Sugiyama, and T. Nakada, "Impact of Heat-Light Soaking and Heat-Bias Soaking on NaF-Treated CIGS Thin Film Solar Cells," *Progress in Photovoltaics: Research and Applications* 27, no. 7 (2019): 623–629, <https://onlinelibrary.wiley.com/doi/abs/10.1002/pip.3135>.
13. S. Ishizuka, H. Shibata, J. Nishinaga, Y. Kamikawa, and P. J. Fons, "Effects of RbF Postdeposition Treatment and Heat-Light Soaking on the Metastable Acceptor Activation of CuInSe₂ Thin Film Photovoltaic Devices," *Applied Physics Letters* 113, no. 6 (2018): 63901, doi:10.1063/1.5031898.
14. J. Chantana, T. Kato, H. Sugimoto, and T. Minemoto, "Enhancement of Photovoltaic Performances of Cu(In,Ga)(S,Se)₂ Solar Cell Through Combination of Heat-Light Soaking and Light Soaking Processes," *Progress in Photovoltaics: Research and Applications* 26, no. 10 (2018): 868–876, eprint: <https://onlinelibrary.wiley.com/doi/abs/10.1002/pip.3031>.
15. J. Chantana, T. Kato, H. Sugimoto, and T. Minemoto, "20% Efficient Zn_{0.9}Mg_{0.1}O:Al/Zn_{0.8}Mg_{0.2}O/Cu(In,Ga)(S,Se)₂ Solar Cell Prepared by All-Dry Process through a Combination of Heat-Light-Soaking and Light-Soaking Processes," *ACS Applied Materials & Interfaces* 10, no. 13 (2018): 11361–11368, Publisher: American Chemical Society, doi:10.1021/acsami.8b01247.
16. J. Nishinaga, T. Nagai, T. Sugaya, H. Shibata, and S. Niki, "Single-Crystal Cu(In,Ga)Se₂ Solar Cells Grown on GaAs Substrates," *Applied Physics Express* 11, no. 8 (2018): 82302, Publisher: IOP Publishing, <https://iopscience.iop.org/article/10.7567/APEX.11.082302/meta>.
17. R. Carron, S. Nishiwaki, S.-C. Yang, et al., "Heat-Light Soaking Treatments for High-Performance CIGS Solar Cells on Flexible Substrates," (2022), In Review, <https://www.researchsquare.com/article/rs-2116168/v1>.
18. S. J. Heise, V. Gerliz, M. S. Hammer, J. Ohland, J. Keller, and I. Hammer-Riedel, "Light-Induced Changes in the Minority Carrier Diffusion Length of Cu(In,Ga)Se₂ Absorber Material," *Solar Energy Materials and Solar Cells* 163 (2017): 270–276, <https://www.sciencedirect.com/science/article/pii/S092702481730051X>.

19. A. Czudek, A. Urbaniak, A. Eslam, R. Wuerz, and M. Igalson, "Dependence of the Magnitude of Persistent Photoconductivity on Sodium Content in Cu(In,Ga)Se₂ Solar Cells and Thin Films," *IEEE Journal of Photovoltaics* 10, no. 6 (2020): 1926–1930, Conference Name: IEEE Journal of Photovoltaics, <https://ieeexplore.ieee.org/document/9171911>.
20. R. Herberhotz, H. W. Schock, U. Rau, et al., "New Aspects of Phase Segregation and Junction Formation in CuInSe/Sub 2/," in *Conference Record of the Twenty Sixth IEEE Photovoltaic Specialists Conference - 1997*, (1997): 323–326, <https://ieeexplore.ieee.org/stampPDF/getPDF.jsp?tp%3D%26arnumber%3D654093%26ref%3DaHR0cHM6Ly9pZjVWVleHBsb3JlmlZlZWUub3JnL2RvY3VtZW50LzY1NDA5Mw%3D%3D%26tag%3D1>.
21. S. Lany and A. Zunger, "Anion Vacancies as a Source of Persistent Photoconductivity in II-VI and Chalcopyrite Semiconductors," *Physical Review B* 72, no. 3 (2005): 35215, <https://link.aps.org/doi/10.1103/PhysRevB.72.035215>.
22. S. Lany and A. Zunger, "Light- and Bias-Induced Metastabilities in Cu(In,Ga)Se₂ Based Solar Cells Caused by the (VSe-VCu) Vacancy Complex," *Journal of Applied Physics* 100, no. 11 (2006): 113725, <https://pubs.aip.org/jap/article/100/11/113725/982506/Light-and-bias-induced-metastabilities-in-Cu-In-Ga>.
23. Y. Sun, S. Lin, W. Li, et al., "Review on Alkali Element Doping in Cu(In,Ga)Se₂ Thin Films and Solar Cells," *Engineering* 3, no. 4 (2017): 452–459, <https://www.sciencedirect.com/science/article/pii/S2095809917306045>.
24. M. Malitckaya, H.-P. Komsa, V. Havu, and M. J. Puska, "Effect of Alkali Metal Atom Doping on the CuInSe₂-Based Solar Cell Absorber," *Journal of Physical Chemistry C* 121, no. 29 (2017): 15516–15528, Publisher: American Chemical Society, doi:10.1021/acs.jpcc.7b03083.
25. J. Pohl and K. Albe, "Intrinsic Point Defects in CuInSe₂ and CuGaSe₂ as Seen via Screened-Exchange Hybrid Density Functional Theory," *Physical Review B* 87, no. 24 (2013): 245203, <https://link.aps.org/doi/10.1103/PhysRevB.87.245203>.
26. P. Pearson, J. Keller, L. Stolt, O. Donzel-Gargand, and C. Platzer Björkman, "Ag-Dependent Behavior Threshold and Metastability in Wide-Gap (Ag,Cu)(In,Ga)Se₂ Solar Cells," *Solar RRL* 8, no. 11 (2024): 2400220, _eprint: <https://onlinelibrary.wiley.com/doi/pdf/10.1002/solr.202400220>.
27. D. Regesch, L. Gütay, J. K. Larsen, et al., "Degradation and Passivation of CuInSe₂," *Applied Physics Letters* 101, no. 11 (2012): 112108, doi:10.1063/1.4752165.
28. S. Siebentritt, T. P. Weiss, M. Sood, M. H. Wolter, A. Lomuscio, and O. Ramirez, "How Photoluminescence Can Predict the Efficiency of Solar Cells," *Journal of Physics: Materials* 4, no. 4 (2021): 42010, <https://iopscience.iop.org/article/10.1088/2515-7639/ac266e>.
29. U. Rau and J. H. Werner, "Radiative Efficiency Limits of Solar Cells With Lateral Band-Gap Fluctuations," *Applied Physics Letters* 84, no. 19 (2004): 3735–3737, <https://pubs.aip.org/apl/article/84/19/3735/510562/Radiative-efficiency-limits-of-solar-cells-with>.
30. D. Abou-Ras, "Microscopic Origins of Radiative Performance Losses in Thin-Film Solar Cells at the Example of (Ag,Cu)(In,Ga)Se₂ Devices," *Journal of Vacuum Science & Technology A* 42, no. 2 (2024): 22803, doi:10.1116/6.0003364.
31. S. Siebentritt, U. Rau, S. Gharabeiki, et al., "Photoluminescence Assessment of Materials for Solar Cell Absorbers," *Faraday Discussions* 239 (2022): 112–129, <https://xlink.rsc.org/?DOI%3DD2FD00057A>.
32. E. Ugur, M. Ledinský, T. G. Allen, J. Holovský, A. Vlk, and S. De Wolf, "Life on the Urbach Edge," *Journal of Physical Chemistry Letters* 13, no. 33 (2022): 7702–7711, Publisher: American Chemical Society.
33. J. H. Werner, J. Mattheis, and U. Rau, "Efficiency Limitations of Polycrystalline Thin Film Solar Cells: Case of Cu(In,Ga)Se₂," *Thin Solid Films* 480–481 (2005): 399–409, <https://www.sciencedirect.com/science/article/pii/S0040609004016128>.
34. D. Abou-Ras, N. Schäfer, C. J. Hages, S. Levchenko, J. Márquez, and T. Unold, "Inhomogeneities in Cu(In,Ga)Se₂ Thin Films for Solar Cells: Band-Gap Versus Potential Fluctuations," *Solar RRL* 2, no. 1 (2018): 1700199, _eprint: <https://onlinelibrary.wiley.com/doi/pdf/10.1002/solr.201700199>.
35. E. M. Spaans, J. de Wild, T. J. Savenije, and B. Vermang, "Unified Potential Fluctuations Model for Photoluminescence Spectra at Room Temperature–Cu(In,Ga)Se₂ Thin Films," *Journal of Applied Physics* 130, no. 12 (2021): 123103, <https://aip.scitation.org/doi/10.1063/5.0056629>.
36. P. Wurfel, "The Chemical Potential of Radiation," *Journal of Physics C: Solid State Physics* 15, no. 18 (1982): 3967, doi:10.1088/0022-3719/15/18/012.
37. R. Carron, C. Andres, E. Avancini, et al., "Bandgap of Thin Film Solar Cell Absorbers: A Comparison of Various Determination Methods," *Thin Solid Films* 669 (2019): 482–486, <https://www.sciencedirect.com/science/article/pii/S0040609018307582>.
38. H. Aboufadi, K. V. Sopiha, J. Keller, et al., "Alkali Dispersion in (Ag,Cu)(In,Ga)Se₂ Thin Film Solar Cells–Insight From Theory and Experiment," *ACS Applied Materials & Interfaces* 13, no. 6 (2021): 7188–7199, <https://pubs.acs.org/doi/10.1021/acsami.0c20539>.
39. M. H. Wolter, R. Carron, E. Avancini, et al., "How Band Tail Recombination Influences the Open-Circuit Voltage of Solar Cells," *Progress in Photovoltaics: Research and Applications* 30, no. 7 (2022): 702–712, _eprint: <https://onlinelibrary.wiley.com/doi/pdf/10.1002/pip.3449>.
40. J. Bisquert, "Unique Curve for the Radiative Photovoltage Deficit Caused by the Urbach Tail," *Journal of Physical Chemistry Letters* 12, no. 32 (2021): 7840–7845, Publisher: American Chemical Society, doi:10.1021/acs.jpcclett.1c01935.
41. A. Nikolaeva, M. Krause, N. Schäfer, et al., "Electrostatic Potential Fluctuations and Light-Soaking Effects in Cu(In,Ga)Se₂ Solar Cells," *Progress in Photovoltaics: Research and Applications* 28, no. 9 (2020): 919–934, _eprint: <https://onlinelibrary.wiley.com/doi/pdf/10.1002/pip.3299>.
42. J. Keller, P. Pearson, N. Shariati Nilsson, O. Stolt, L. Stolt, and M. Edoff, "Performance Limitations of Wide-Gap (Ag,Cu)(In,Ga)Se₂ Thin-Film Solar Cells," *Solar RRL* 5, no. 9 (2021): 2100403, <https://onlinelibrary.wiley.com/doi/abs/10.1002/solr.202100403>.
43. R. K. Ahrenkiel, D. H. Levi, S. Johnston, W. Song, D. Mao, and A. Fischer, "Photoconductive Lifetime of CdS Used in Thin-Film Solar Cells," in *Conference Record of the Twenty Sixth IEEE Photovoltaic Specialists Conference - 1997*, (IEEE, 1997): 535–538, <http://ieeexplore.ieee.org/document/654146/>.
44. H. Yin, A. Akey, and R. Jaramillo, "Large and Persistent Photoconductivity due to Hole-Hole Correlation in CdS," *Physical Review Materials* 2, no. 8 (2018): 84602, <https://link.aps.org/doi/10.1103/PhysRevMaterials.2.084602>.
45. P. Pearson, J. Keller, L. Stolt, M. Edoff, and C. Platzer Björkman, "The Effect of Absorber Stoichiometry on the Stability of Widegap (Ag,Cu)(In,Ga)Se₂ Solar Cells," *Physica Status Solidi (b)* 259, no. 11 (2022): 2200104, _eprint: <https://onlinelibrary.wiley.com/doi/pdf/10.1002/pssb.202200104>.

Supporting Information

Additional supporting information can be found online in the Supporting Information section.